Geoderma 319 (2018) 132–141

Contents lists available at ScienceDirect

Geoderma

journal homepage: www.elsevier.com/locate/geoderma

# Quantitative analysis of wetting front instabilities in soil caused by treated waste water irrigation

Frederic Leuther[a,*], Ulrich Weller[a], Rony Wallach[b], Hans-Jörg Vogel[a,c]

[a] Department of Soil Physics, Helmholtz Centre for Environmental Research — UFZ, Theodor-Lieser Str. 4, Halle (Saale) 06120, Germany
[b] Department of Soil and Water Sciences, The Hebrew University of Jerusalem, Rehovot, Israel
[c] Soil Sciences, Martin-Luther-University Halle-Wittenberg, Halle (Saale), Germany

ARTICLE INFO

Handling Editor: Christine L.S. Morgan

*Keywords:*
Soil water repellency
Treated waste water irrigation
Unstable flow
Preferential flow
Water infiltration
X-ray analysis

ABSTRACT

Irrigation with treated waste water (TWW) is a common practice in agriculture, mainly in arid and semiarid areas as it provides a sustainable water resource available at all-season in general and at freshwater shortage in particular. However, TWW still contains abundant organic material which is known to decrease soil wettability, which in turn may promote flow instabilities that lead to the formation of preferential flow paths. We investigate the impact of long-term TWW irrigation on water wettability and infiltration into undisturbed soil cores from two commercially used orchards in Israel. Changes of water content during infiltration were quantitatively analysed by X-ray radiography. One orchard (sandy clay loam) had been irrigated with TWW for more than thirty years. In the other orchard (loamy sand) irrigation had been changed from freshwater to TWW in 2008 and switched back in some experimental plots to freshwater in 2012. Undisturbed soil cores were taken at the end of the dry and the rainy season to investigate the seasonal effect on water repellency and on infiltration dynamics in the laboratory. The irrigation experiments were done on field moist samples. A test series with different initial water contents was run to detect the influence on water movement at different wettabilities. In this study we show that the infiltration front stability is dependent on the history of waste water irrigation at the respective site and on the initial water content.

## 1. Introduction

Crop irrigation with treated waste water has become a common practice in arid and semiarid areas to deal with water scarcity and to reduce the usage of fresh water. In Israel, the reuse of former waste water already provides more than 50% of total water consumption by agriculture (OECD, 2015). Besides the advantages as a sustainable water resource and recycling of nutrients, it has been observed that TWW irrigation may have critical impact on soil hydrological properties mainly induced by the load of organic compounds (DeBano, 1981; Doerr et al., 2000; Wallach et al., 2005). A reduced affinity of soil to water, so called soil water repellency, may lead to reduced infiltration capacities, intensify overland flow, and formation of preferential flow paths that render the spatial wetting pattern uneven (Rahav et al., 2017). Previous studies have shown these effects as a result of forest fires, decomposing of litter from plants rich in lipids and waxes, root exudates, fungal hyphae, and the usage of irrigation water of poor quality (Bughici and Wallach, 2016; Dekker and Ritsema, 2000; Horne and McIntosh, 2000; Lado and Ben-Hur, 2009; Zavala et al., 2009), concluding that mainly hydrophobic organics influences soil hydraulic properties. The occurrence of water repellency is induced by hydrophobic molecules coating mineral surfaces and by the presence of hydrophobic particles in the pore space (Doerr et al., 2000). The hydrophobic effect of amphipathic coatings depends on soil water content as their non-polar hydrocarbon chains are changing the orientation during drying. Hydrophobicity of soil can become a persistent attribute over time when supply is larger than degradation or leaching of these substances. The occurrence of water repellency and their affect on soil water dynamics is still not fully understood (Doerr et al., 2007). One reason is that the detection of wetting front characteristics and, furthermore, quantifying preferential flow in undisturbed soils is a challenge (Allaire et al., 2009). Therefore, infiltration studies in the past were mainly carried out by using flat, quasi two-dimensional Hele-Shaw cells (Carrillo et al., 2000; Rye and Smettem, 2017; Wallach and Jortzick, 2008; Wang et al., 2000; Xiong et al., 2012), by detecting wetting pattern of soil profiles and transects (Dekker and Ritsema, 1994; Kobayashi and Shimizu, 2007; Lipsius and Mooney, 2006), or by solute transport experiments (Clothier et al., 2000). The impact of water repellency on the wetting behaviour of the soil and the occurrence of preferential flow is already described, but is mainly limited to

* Corresponding author.
*E-mail address:* frederic.leuther@ufz.de (F. Leuther).

https://doi.org/10.1016/j.geoderma.2018.01.004
Received 20 September 2017; Received in revised form 12 December 2017; Accepted 4 January 2018
Available online 02 February 2018

two-dimensional detection of a three-dimensional process, to a single scenario in the field by destroying the structure, or to point measurements. Rahav et al. (2017) have shown the occurrence of uneven wetting and preferential flow on the field scale via non-invasive ERT-measurements. A new approach developed by Weller et al. (2017) enables a direct, non-destructive quantification of water infiltration into undisturbed soil cores via X-ray radiography without the usage of chemical tracers. Compared to X-ray computer tomography image recoding takes only seconds, this enables the detection of fast moving water fronts. The results are 2D projections of mean changes in water content along the beam line, i.e. the horizontal sample depth. The objective of this study was to use this method to investigate influences of long-term TWW irrigation on the stability of infiltration fronts in undisturbed, cylindrical soil cores under different moisture conditions and, therefore, simulate diverse irrigation strategies. Furthermore, we included seasonal dynamics and soil textural differences to test for persistence of repellency, and the effect of reclaiming of water repellent soil by fresh water irrigation.

## 2. Materials & methods

### 2.1. Study sites and soil sampling

The study sites were located in Israel's coastal plain which is dominated by brown-red (degrading) sandy soils and marked by two pronounced climate seasons, a hot and dry summer where orchards are irrigated, and a rainy winter without irrigation. The first sampling location was close to Rehovot, where soil texture is loamy sand (denoted in the following as S). Here, three different treatments of irrigation were investigated: fresh water (FW), treated waste water (TWW), and no irrigation (NoI). Bulk density and carbon content were different in the irrigated parts ($\rho_b = 1.31$ g cm$^{-3}$, $C = 1.2\%$) compared to the non-irrigated part ($\rho_b = 1.64$ g cm$^{-3}$, $C = 0.6\%$), shown in Table 1. Soil pH under TWW irrigation ($pH = 5.7$) was reduced compared to NoI ($pH = 7.4$) and FW irrigation ($pH = 7.2$). The second location was close to Hadera, where sandy clay loam (denoted in the following as L) was the predominant soil texture. At this site, no freshwater irrigation was available, only treated waste water (TWW) and no irrigation (NoI). Bulk density $\rho_b = 1.48$ g cm$^{-3}$ and soil $pH = 7.4$ were independent of the irrigation regime. The carbon content under NoI $C = 1.7\%$ was higher than under TWW irrigation $C = 0.8\%$ (Table 1). At both study sites, citrus fruit (grapefruit in Rehovot and mandarin in Hadera) were produced. Soil cultivation was mainly reduced to inorganic fertilization without any tillage. In Rehovot, the water management was changed from fresh water to secondary treated waste water irrigation in 2008. In 2012, single plots of a block design experiment were converted to ground water irrigation for soil reclamation (Rahav et al., 2017). In Hadera, farmers have used secondary treated waste water for more than 30 years. At both study sites, the amount of irrigation was adjusted to the daily evapotranspiration rates. The first sampling was done at the end of dry season (October 2015), when soils were irrigated with the different treatments for seven months. The second campaign was scheduled in February 2016, after four months of the rainy season without irrigation. The samples were taken within the wet soil along the dripper lines (FW and TWW) and between the tree rows beyond the reach of irrigation water (NoI). Soil cores were sampled from the topsoil (0 mm to 200 mm depth) by using a custom-made drill (UGT GmbH, Germany) for undisturbed sampling of cylindrical soil cores (Kuka et al., 2013). The sample cylinders were made of polycarbonate with a wall thickness of 3 mm and an outer diameter of 100 mm. Depending on the difficulty to take undisturbed samples below the trees we used columns of different height, 100 mm and 200 mm. The samples were immediately stored in plastic bags to keep them field moist, carefully packed and shipped to Germany. Overall, 13 minimally disturbed soil cores (2 S-FW, 4 S-NoI, 2 S-TWW, 5 L-TWW) were taken in October 2015 and 23 (5 S-FW, 1 S-NoI, 6 S-TWW, 4 L-TWW, 7 L-NoI) in February 2016. Additional 77 undisturbed samples (50 mm in diameter and 50 mm in height) were taken from the topsoil in the vicinity of larger soil cores to test the soil for water repellency.

**Table 1**
Site conditions: texture (FAO, LS = loamy sand, SCL = sandy clay loam), grain size distribution, bulk density, soil $pH_{H_2O}$, and carbon content ($C$).

| Treatment | Texture | Sand | Silt | Clay | Bulk density | pH | C |
|---|---|---|---|---|---|---|---|
| S-NoI | LS | 81.4% | 7.8% | 10.8% | 1.64 g cm$^{-3}$ | 7.4 | 0.6% |
| S-FW | LS | 80.7% | 8.5% | 11.1% | 1.31 g cm$^{-3}$ | 7.2 | 1.2% |
| S-TWW | LS | 86.2% | 5.9% | 7.9% | 1.32 g cm$^{-3}$ | 5.7 | 1.2% |
| L-NoI | SCL | 63.4% | 14.3% | 22.3% | 1.48 g cm$^{-3}$ | 7.5 | 1.7% |
| L-TWW | SCL | 65.5% | 12.6% | 21.8% | 1.48 g cm$^{-3}$ | 7.4 | 0.8% |

### 2.2. Soil water repellency

The persistence and intensity of soil water repellency was characterized by two methods, the water drop penetration time test (WDPT) (Doerr, 1998; Letey et al., 2000) and the sessile drop contact angle (CA) (Bachmann et al., 2000). The small (50 mm in diameter) undisturbed soil samples were placed in an oven at 50 ° C until a reference water content corresponding to that of air dried soil was reached. WDPT and CA were measured for the upper 50 mm of the soil in an interval of 10 mm following Bughici and Wallach (2016). The WDPT was determined by placing three drops of 50 µL distilled water on the soil surface and recording the required time for their complete infiltration. The average time was used to classify their water repellency (Bisdom et al., 1993): class I, not water repellent (infiltration within 5 s); class II, slightly water repellent ($5 < \text{WDPT} \leq 60$ s); class III, strongly water repellent ($60 < \text{WDPT} \leq 600$ s); class IV, severely water repellent ($600 < \text{WDPT} \leq 3600$ s); class V, extremely water repellent (WDPT $> 3600$ s). The initial contact angle and its variation in time was measured with a goniometer (EasyDrop DSA20E, KRÜSS GmbH, Germany) for a flat surface of air dried, sieved soil ( $< 50$ µm) from every 10 mm layer. The soil was glued to a double-sided tape attached to a pathology slide to form a flat single layer of soil particles and a drop volume of 15 µL was placed on the single particle layer. The change in drop shape was translated to a change in CA by the Easy Drop Software. The decrease in CA during the contact time $\phi(t)$ of the liquid with soil particles can be influenced by conformational changes, hydration, or rearrangement of organic molecules, coating soil-particle surfaces as a result of contact with water (Graber et al., 2007). Double-exponential-decrease functions were fitted to describe the dynamics of changing CA (Eq. (1)), as an additional quantification of water repellency persistence.

$$\phi(t) = a^{*}e^{-b*t} + c^{*}e^{-d*t} \quad (1)$$

where $b$, and $d$ represents the rate at which the CA ($a + c$) varies with time ($t$). The sum of parameter $a$ and $c$ at time point zero is the initial CA, and their ratio describes the relevant dominance of the tailing.

### 2.3. Infiltration experiments

The detection of infiltration fronts in the larger cylindrical, undisturbed soil cores followed the approach developed by Weller et al. (2017). 36 samples were tested for their infiltration characteristics while they were still field moist. Afterwards, a test series with 12 loamy sand samples (6 TWW and 6 FW) at reduced initial soil water content was investigated. Therefore, soil cores were dried in an oven at 50 ° C for three and for seven days. All irrigation experiments were performed inside an X-ray microtomograph (Nikon Metrology X-Tek XCT 225) with the same irrigation rate (Fig. 1 *a*). A peristaltic pump provided a constant flux of $j = 8$ mm h$^{-1}$ which was equally distributed over the soil surface by an irrigation device with 21 needles installed on top of the sample. The applied flux correspond to the irrigation rate of one

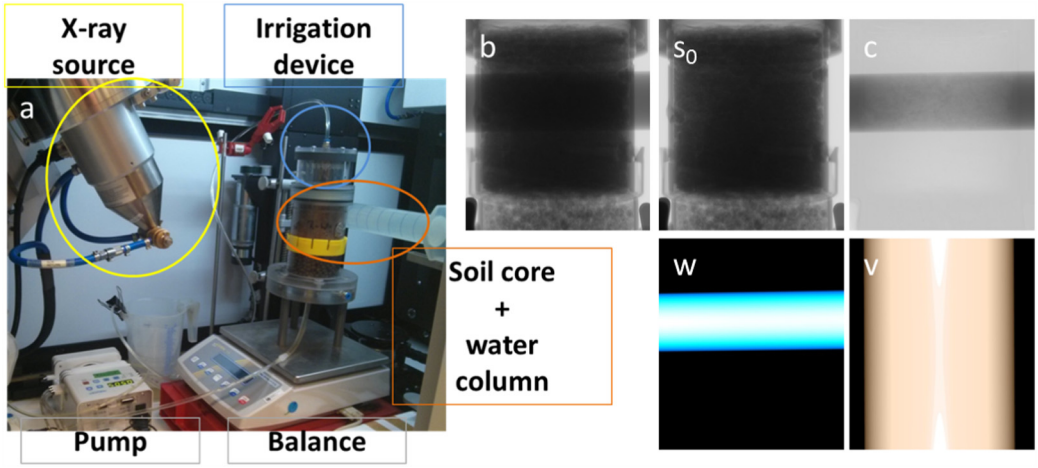


**Fig. 1.** Workflow of water quantification: *a*) experimental set-up inside X-ray microtomograph *b*) radiography of initial soil plus water column $s_0$) radiography of initial soil column *c*) water attenuation *w*) projected water column *v*) projected soil column.

**Table 2**
Soil specific fitting parameters.

| Fitting parameter | $h_1$ | $h_2$ | $h_3$ |
|---|---|---|---|
| Loamy sand | $3.26 \times 10^{-5}$ | $5.95 \times 10^{-2}$ | $-2.78 \times 10^{-4}$ |
| Sandy clay loam | $4.98 \times 10^{-5}$ | $9.02 \times 10^{-2}$ | $-2.70 \times 10^{-4}$ |

dripper in the field. To prevent effects on soil chemistry and structure, like dispersion of clay minerals, the salt concentrations of the irrigation water were adapted to the field specific water characteristics (S-FW $EC = 857$ µS cm$^{-1}$, S-TWW $EC = 1735$ µS cm$^{-1}$, and L-TWW $EC = 1386$ µS cm$^{-1}$). At the lower boundary, two different experimental set-ups were chosen for the field moist samples and the dryer series.

### 2.3.1. Field moist samples

At the lower boundary a prescribed matrix potential was applied through a pressure control system via a ceramic plate. Therefore, matrix potentials were monitored by two tensiometers installed along the vertical profile at 25 mm and 75 mm depth. By adapting the lower boundary to the potential measured by the topmost tensiometer, the flow conditions were forced towards gravity-flow (Weller and Vogel, 2012). The outflow was removed immediately using the same pump as for the irrigation system. To independently measure the total change in water content during infiltration, the entire experimental set-up was mounted on a balance and the mass was automatically recorded every 20 s. The experiments were stopped when total mass remained constant, assuming that an equilibrium of outflow and inflow was reached and a stable flow field was established inside the column.

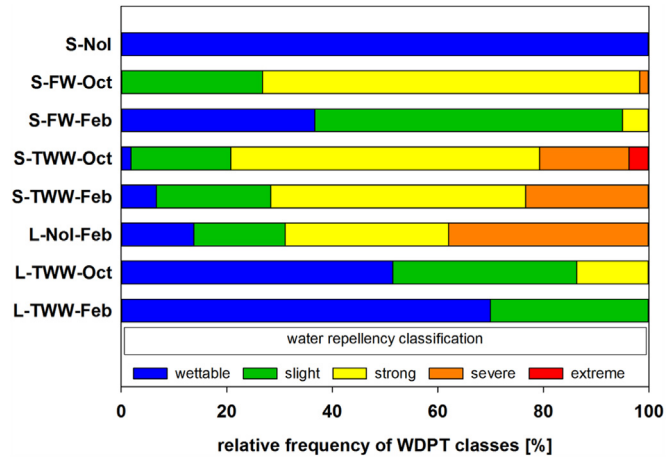


**Fig. 2.** Relative frequency of water drop penetration time (WDPT) classes for the top soil (0 mm to −50 mm) of different treatments.

**Table 3**
Median WDPT classes for single layers of the top soil (0 mm to −50 mm).

| Depth | 0 cm | −20 mm | −30 mm | −40 mm | −50 mm |
|---|---|---|---|---|---|
| S-NoI | 1.0 | 1.0 | 1.0 | 1.0 | 1.0 |
| S-FW Oct | 2.0 | 3.0 | 3.0 | 3.0 | 3.0 |
| S-FW Feb | 1.0 | 2.0 | 2.0 | 2.0 | 2.0 |
| S-TWW Oct | 3.0 | 3.0 | 3.0 | 3.0 | 3.0 |
| S-TWW Feb | 3.0 | 3.0 | 3.0 | 3.0 | 3.0 |
| L-NoI Feb | 3.5 | 4.0 | 3.0 | 2.5 | 1.0 |
| L-TWW Oct | 2.0 | 1.0 | 1.0 | 2.0 | 1.0 |
| L-TWW Feb | 2.0 | 1.0 | 1.0 | 1.0 | 1.0 |

### 2.3.2. Dry initial conditions

The set-up for the dried soil samples was slightly different as the pressure control system could not be used due to the low water potential. The tensiometers were removed and the lower boundary was changed to free drainage conditions (seepage boundary). Therefore, the cylindrical samples were covered with a perforated lid to stabilize the core and placed on a funnel-shaped support which was filled with saturated foamed clay pellets.

Radiographs were taken with different, soil specific energy settings and copper filters to gain a wide grey value distribution: loamy sand 140 keV, 470 µA, and 1.5 mm copper filter, and sandy clay loam 160 keV, 520 µA, and 2.0 mm copper filter. The temporal progress of the fronts were repeatedly captured via constant imaging of radiograms at time steps of 150 s to 600 s by averaging 16 frames with an exposure time of 1 frame per second. Latency of the detector panel can cause artificial grey value drifts during the experiments which impairs the quantification of water movement. To reduce this effect, the radiation source was switched off in between two records and 2 reference copper discs (loamy sand: 1.5 mm and 11 mm, sandy clay loam: 2.0 mm and 14 mm) were installed next to the samples to correct the images by a linear interpolation between the grey value drifts of the discs.

## 2.4. Quantification of water infiltration

Infiltrating water was quantified as 2D projections of the mean changes in water content along the beam line for every pixel following the work-flow developed by Weller et al. (2017). The method is based on a direct, soil specific calibration of grey values for the full range of soil and water content. Therefore, a radiography was required with an additional water column (radius of 27 mm) mounted perpendicular to the soil column in the background of the sample to calibrate the method before starting the irrigation experiment (Fig. 1*b*). This projection

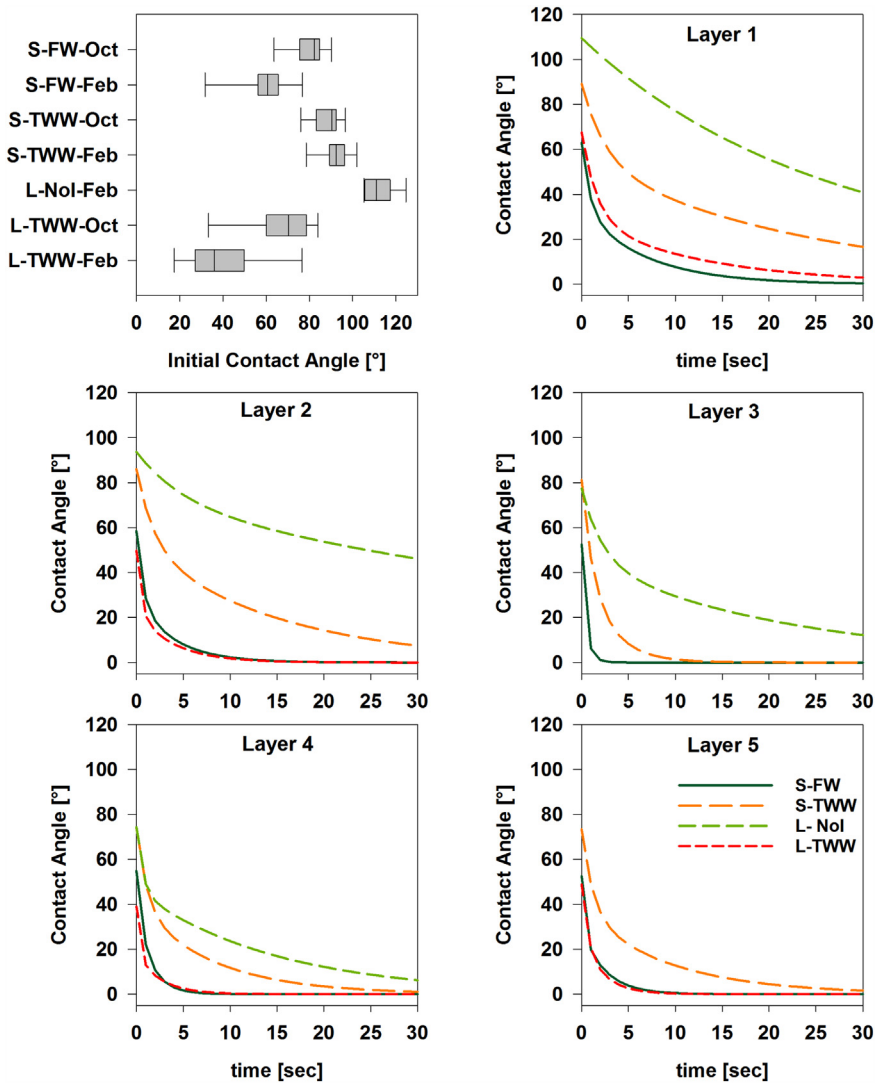


**Fig. 3.** Initial CA at soil surface (top left) and averaged dynamic CA-fit for single layers of the top soil (0 mm to − 50 mm).

provides a broad range of defined water contents because of the cylindrical form of both columns: a water gradient in vertical direction and a soil gradient in horizontal direction. At first, cylindrical projections for the water and soil column were created to store the information of the specific spatial paths length of radiation in an image file (Fig. 1*w* and *v*). The attenuation caused by different water contents was obtained by a division of the radiographs with and without the water column (Fig. 1*c*). A pixel-wise point data sampling of the projected water column (*w*), the initial soil column ($s_0$) and the value of water attenuation (*c*) were used to determine the sample specific variables $h_1$, $h_2$, and $h_3$ of the hyperbola e function (Eq. (2)).

$$c = e^{w\left(\frac{h_1}{(s_0+h_2)}+h_3\right)}. \quad (2)$$

Before calculating the change in water content for every single time step, the radiographs were corrected for the grey value drift due to panel latency by linear interpolation between the drifts of the two copper discs. Finally, the change in water content ($w_t$) was determined as an integral along the beam line using Eq. (3), where $s_t$ denotes the grey value for the single time step, and $s_d$ the drift corrected initial grey value. The translation into volumetric water content was done by dividing the calculated water image by the projection length of the soil column (*v*).

$$w_t = \frac{\ln\left(\frac{s_t}{s_d}\right)}{\left(\frac{h_1}{(s_d+h_2)}+h_3\right)}. \quad (3)$$

This method was developed only after the irrigation experiments for field-moist samples from the first sampling campaign. For these samples the radiographs including the calibration based on the water column was not available. Therefore, a sample specific determination of the variables in Eq. (2) was not possible. Instead, mean values of soil specific fitting parameters determined from the second sampling campaign were used (Table 2). For each time step, the average change in water content for the entire sample projection as calculated by image analysis was verified by comparison to the changes in total mass recorded by the balance.

The projections were analysed in a 16 bit format were the maximum value (65,535) corresponds to a change in water content, $\Delta\theta$ of 66 vol %. Hence, we rescaled the values to a range between 0 vol % to 66 vol %. To illustrate the change in water content we used a continuous colour code where blue refers to small and yellow to large changes, while black equals no change. The spatial resolution is 0.065 mm per pixel and their values are mean changes $\Delta\theta$ along the beam line. Disturbances at the lower part of the single images were due to the experimental set-up. Movements of a bolt or the socket caused artefacts which were detected as changes in water content. Therefore, the values of the lower 20 mm were not considered in analyses of the infiltration

**Table 4**
Averaged fitting parameters for single layers of the top soil (0 mm to − 50 mm). Values in parenthesis are coefficient of variation.

| Parameter | Depth [cm] | S-FW | S-TWW | L-NoI | L-TWW |
|---|---|---|---|---|---|
| a | 0.0–1.0 | 29.5 (0.2) | 34.7 (0.2) | 45.0 (0.7) | 38.7 (0.2) |
| b | 0.0–1.0 | 1.18 (0.8) | 0.39 (1.3) | 0.05 (0.8) | 0.62 (0.6) |
| c | 0.0–1.0 | 33.4 (0.3) | 54.4 (0.1) | 64.5 (0.5) | 28.8 (0.2) |
| d | 0.0–1.0 | 0.15 (0.9) | 0.04 (1.6) | 0.02 (2.1) | 0.08 (0.6) |
| $\phi_0 = 0/n$ | 0.0–1.0 | 0/12 | 0/12 | 0/6 | 2/16 |
| a | 1.0– 2.0 | 30.1 (0.2) | 33.7 (0.2) | 22.2 (0.3) | 27.2 (0.5) |
| b | 1.0–2.0 | 1.55 (0.9) | 0.54 (1.4) | 0.20 (0.7) | 2.17 (1.1) |
| c | 1.0–2.0 | 28.3 (0.3) | 52.3 (0.2) | 71.5 (0.3) | 22.6 (0.3) |
| d | 1.0–2.0 | 0.25 (1.0) | 0.07 (1.4) | 0.01 (1.2) | 0.26 (0.9) |
| $\phi_0 = 0/n$ | 1.0–2.0 | 0/12 | 0/12 | 0/6 | 5/16 |
| a | 2.0–3.0 | 26.2 (0.5) | 34.8 (0.3) | 32.5 (0.2) | NaN |
| b | 2.0–3.0 | 3.19 (1.0) | 0.91 (1.9) | 0.44 (1.1) | NaN |
| c | 2.0–3.0 | 26.3 (0.6) | 46.3 (0.3) | 44.9 (0.5) | NaN |
| d | 2.0–3.0 | 1.64 (2.5) | 0.35 (2.4) | 0.04 (1.2) | NaN |
| $\phi_0 = 0/n$ | 2.0–3.0 | 0/12 | 0/12 | 0/6 | 7/16 |
| a | 3.0–4.0 | 22.1 (0.7) | 34.5 (0.3) | 28.4 (0.8) | 20.6 (0.6) |
| b | 3.0–4.0 | 1.71 (11.6) | 0.95 (1.1) | 1.55 (1.5) | 3.57 (1.3) |
| c | 3.0–4.0 | 32.7 (0.4) | 39.6 (0.3) | 45.9 (0.4) | 18.4 (0.7) |
| d | 3.0–4.0 | 0.60 (3.2) | 0.12 (1.2) | 0.07 (1.3) | 0.40 (1.2) |
| $\phi_0 = 0/n$ | 3.0–4.0 | 1/12 | 0/12 | 2/6 | 12/16 |
| a | 4.0–5.0 | 23.6 (0.4) | 36.7 (0.3) | NaN | 23.2 (1.1) |
| b | 4.0–5.0 | 3.93 (0.9) | 0.83 (1.0) | NaN | 1.69 (0.9) |
| c | 4.0–5.0 | 28.9 (0.4) | 36.6 (0.5) | NaN | 25.6 (0.5) |
| d | 4.0–5.0 | 0.40 (1.0) | 0.11 (1.4) | NaN | 0.46 (1.3) |
| $\phi_0 = 0/n$ | 4.0–5.0 | 1/12 | 0/12 | 5/6 | 13/16 |

characteristics. Furthermore, it should be noticed that the projections are more sensitive to detect preferential flow at the edges of the projected cylindrical body as the averaged soil volume is smaller. To quantify patterns of water infiltration, a statistical description of the projected flow field at the end of experiments was done. Specifically, the change in water content $\overline{\Delta\theta}$ and its standard deviation, *sd*, was measured for a squared area of 40,000 pixels where water flow was detected. A threshold of $\overline{\Delta\theta} - 3{*}sd$ was used to divide the images into areas with and without detected water flow.

## 3. Results

### 3.1. Soil water repellency

WDPT greater than 5 s were detected for all sampling locations except for the non-irrigated part of the loamy sand, indicating marks of water repellency. Fig. 2 presents the WDPT classifications for the topsoil (0 mm to −50 mm) of the different locations, treatments, and seasons. Table 3 lists the median WDPT-class for the single layers. For the loamy sand, most FW soil samples were classified as slightly to strongly water repellent and TWW samples as slightly to severely water repellent. Including seasonal dynamics, a reduction of WDPT at the end of the rainy season was detected at the FW irrigated plots, while repellency stayed high under TWW irrigation. In February, most FW samples were classified as not to slightly water repellent, TWW samples as slightly to severely water repellent. For all loamy sand samples water repellency was not changing with depth, independent of the season. For the sandy clay loam, the irrigated samples were mostly classified as not to slightly water repellent. Only after the dry season 14% of the measurements conducted at TWW samples were classified as strongly water repellent. Samples taken from the non-irrigated parts provided a wide range from not to severely water repellent. This wide spread of classes was also detected for individual layers. L-NoI was the only treatment where WDPT decreased with depth.

The initial contact angles (CA) of the soil surfaces provide similar results in terms of water repellency distribution (Fig. 3, top left). Except for NoI of the loamy sand, all measured CA were above 0° and therefore classified as sub-critical water repellent ( < 90°) and water repellent (≥ 90°). To compare the different treatments statistically, an analysis of the initial contact angles measured at the soil surfaces were done by testing Tukey Honestly Significant Differences with a 95% family-wise confidence level. For the loamy sand, there was a statistical significant ($p < .001$) decrease of CA from S-FW October (mean CA 79.8° with a standard deviation of ± 8.6) to S-FW February (59.0° ± 13.4) and no significant difference between S-TWW Oct (88.7° ± 6.5) and S-TWW Feb (91.9° ± 7.2). Comparing between the irrigated treatments, CA measured in February were significantly higher at TWW-irrigated plots compared to FW-irrigated plots, but no differences in October. For the sandy clay loam, a significant decrease of CA was determined for L-TWW between the two sampling occasions, the mean CA for October was 67.0° ± 16.4 and for February 39.7° ± 19.3. Furthermore, the CA at the soil surface of the non-irrigated part (112.1° ± 7.1) was significantly higher compared to the irrigated part, and overall the highest.

The parameters of the fitted double-exponential-decrease functions of changing CA, $\phi(t)$, with time are presented in Table 4. Residuals of the measurements provided an $R^2$ to evaluate the quality of the fit. The mean values and standard errors were determined for all replications where $R^2$ was larger than 0.75 and used to plot the decrease in CA with contact time for the different treatments and depths from 0 mm to − 50 mm (Fig. 3). Missing values in layer 3 (L-TWW) are due to insufficient qualities of the fits and in layer 5 (L-NoI) due to the wettability of the soil. The rate of decreasing CA (*b*) was lowest on the top layers for all treatments. For the loamy sand, the rate of decrease for FW soil was two to four times larger than for the TWW soil, especially in − 40 mm to − 50 mm depth. For the sandy clay loam, the rate of decrease for the L-TWW was two to ten times larger than for L-NoI. Overall, L-NoI provided the lowest decrease in CA, but *b* was increasing with depth and complete wettability was reached in layer 5.

### 3.2. Infiltration front at field moisture

The propagation of water infiltration in 20 field moist samples from Rehovot (7 × S-FW, 8 × S-TWW, 5 × S-NoI) and 10 samples from Hadera (7 × L-TWW, 3 × L-NoI) were successfully determined. The detection of mean changes in water content, $\Delta\theta$, along the sample profile via radiography were confirmed by the recorded mass data. In October, samples of irrigated areas (TWW and FW) were taken during or shortly after the daily irrigation while in February the soils were still moist from rain. Therefore, the initial water contents were close to field capacity and changes due to infiltrating water consequently low. In Rehovot (loamy sand), the mean initial water contents of FW and TWW-irrigated samples were about 25 vol % and of NoI-samples about 18 vol %. When saturated, the maximum water holding capacity of the topsoil at FW/TWW plots is 42 vol % and at NoI 34 vol %. The constant irrigation rate of $j = 8$ mm $h^{-1}$ increased the water content for irrigated samples by 7 vol % and 11 vol % for NoI. In Hadera (sandy clay loam), the sampled soil under the drippers contained 29 vol % of water and the non-irrigated part 21 vol %. $\Delta\theta$ was about 6 vol % for TWW samples and 9 vol % for NoI. The maximum water holding capacity of the topsoil in the irrigated part is 38 vol %, and 31 vol % between the tree rows. Here, the samples were close to saturation at the end of experiment. Fig. 4 shows the calculated projections of changes in water content, $\Delta\theta$, due to infiltrating water as a time series (rows) of one representative sample of each treatment and location (columns). The results of all infiltration experiments are provided in the supplementary material (s.m.).

For the loamy sand (S, Figs. A.9, and A.10, s.m.), infiltration fronts were clearly detectable and water was infiltrating homogeneously, independent of treatment (FW, TWW, NoI) and season (Oct = dry, Feb = rainy season). After 60 min to 80 min of irrigation the infiltration fronts had passed the samples and water contents had increased uniformly from top to the bottom. Projections of samples H, K, L, and N provided a drift in $\Delta\theta$ along the vertical profile from 6 vol % to 1 vol %,

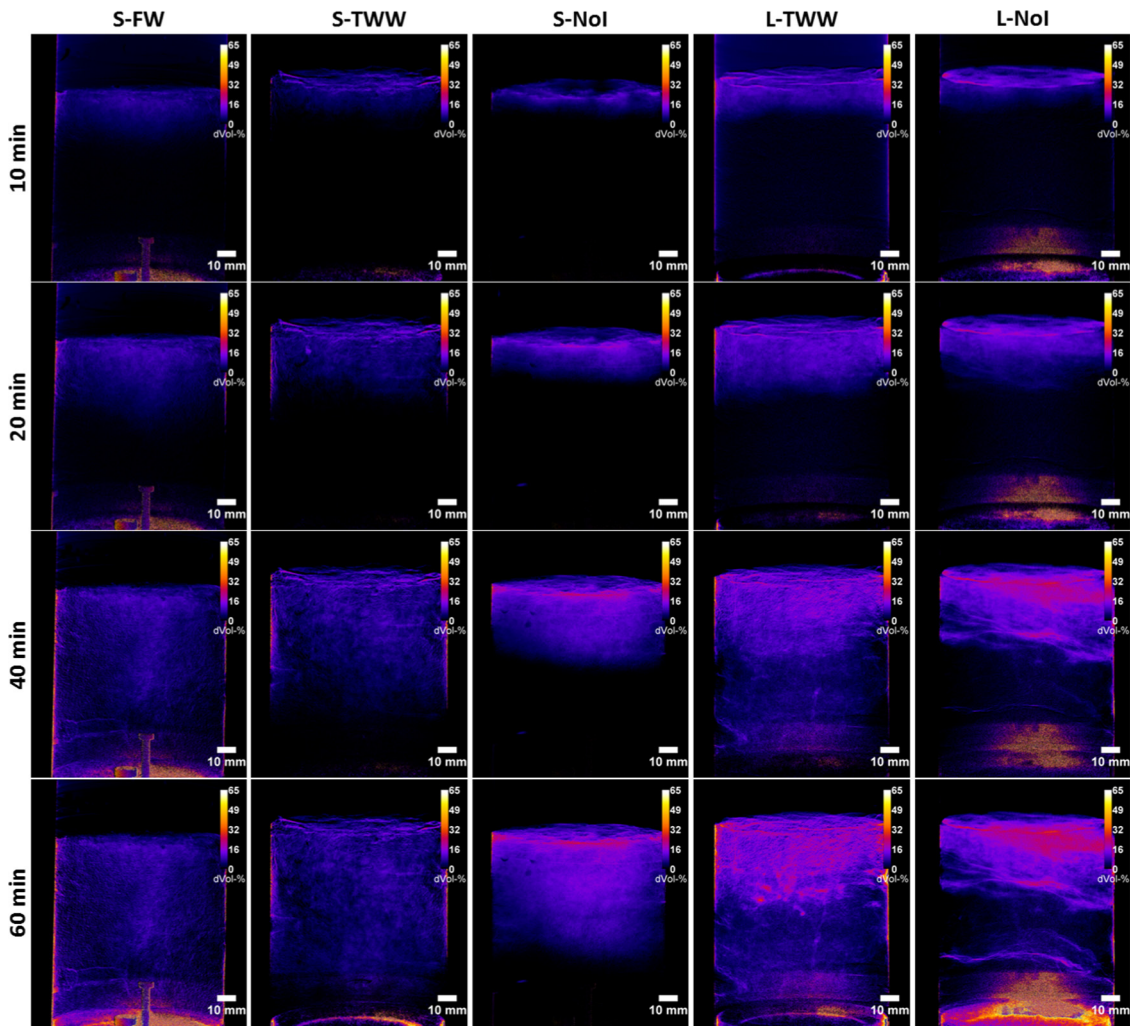


**Fig. 4.** Changes in water content $\Delta\theta$ (vol %) during infiltration experiments. Columns separate samples from different location/treatment. From left to right: Rehovot S-FW, S-TWW, S-NoI and Hadera L-TWW, and L-NoI. Rows illustrate the progress of infiltrating water in time: after 10 min, 20 min, 40 min, and 60 min of irrigation.

furthermore areas with low change in water contents were detected, especially in the lower parts. At sample J, a layer of 30 mm in height, starting 20 mm under the sample surface, was determined where water content did not change, an increase was detected only for single pathways. Sample P also provided a layer of 40 mm with higher increase of $\Delta\theta$, located at the sample top, but the measurement was biased by an experimental error where a constant lower boundary of − 350 hPa was applied. Nevertheless, also here the infiltration front propagated uniformly.

For the sandy clay loam (L, Fig. A.11), samples from the TWW-irrigated plots show similar results as water was infiltrating homogeneously along the entire sample projection. No larger areas without changes in water contents were detected, independent of the season. At the surfaces of samples A, B, and C thin layers of high change in water content (30 vol % to 65 vol %) were captured after 40 min due to ponding of water. In contrast to the irrigated area, NoI samples provided slight heterogeneities in $\Delta\theta$. Patterns of lower changes in water content were distributed over the samples projections and a gradient of larger $\Delta\theta$ from the top to lower changes at the bottom was detected. Furthermore, layering of $\Delta\theta$ was observed for samples H and J. After 60 min of irrigation, at most areas of the samples a change in water content was detected.

### 3.3. Infiltration front at reduced initial water content

The reduced initial water content had a significant effect on the observed flow fields. Three days of drying reduced the initial water content of the loamy sand to 13 vol % and after seven days to 1.5 vol %. It should be noticed that this water was not equally distributed due to small-scale heterogeneities in hydraulic properties. Fig. 5 shows the results of the different infiltration experiments for the same two samples presented already in Fig. 4. Fig. 6 shows the associated relative changes in water content over time detected via gravimetric data. Projections of all experiments are attached in the supplementary material. As water was infiltrating slower due to increasing $\Delta\theta$, the presented time series were adjusted to the infiltration front propagation. After three days of drying, water was infiltrating the FW samples mostly uniform from top to bottom (Fig. A.12, s.m.). An exception is sample E, where water flow was concentrated at one side. Samples A, B, and G show a gradient in change of water content from top (high) to bottom (low), due to the initial conditions with a high gradient of water loss from the sample top (dry) to the bottom (moist). At the end of experiments changes in water content were detected over the entire FW samples. In contrast, preferential flow was observed for all samples of the TWW treatment, except for sample H. Single pathways conducted the water from top to the lower boundary, where it spread. Subsequently samples were wetted from both, the top and bottom. At the end of experiments, when water inflow and outflow was equilibrated, water content was increased in most parts of the samples with exception in I, L, and N. The gravimetric data (Fig. 6) confirm the observed changes in water flow due to the drying process. While relative changes in water content for S-FW was systematically increasing with drying time, the

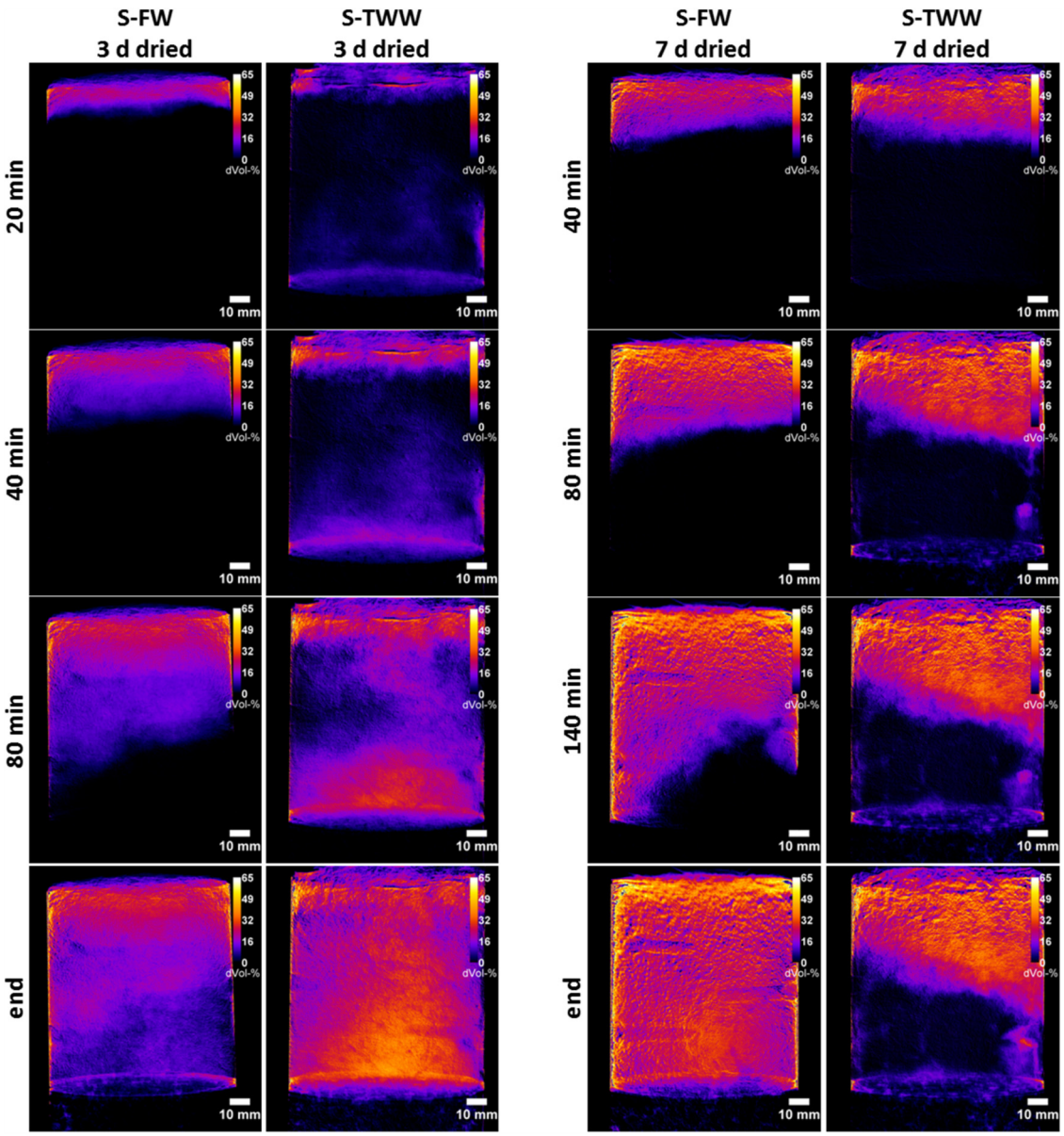


**Fig. 5.** Changes in water content $\Delta\theta$ (vol %) during infiltration experiments of dried samples (50 ° C). On the left side: S-FW and S-TWW dried for three days. On the right side: same S-FW and S-TWW samples dried for 7 days.

change in water content for S-TWW was lower after seven days of drying than after three days of drying.

After seven days of drying, the differences between the treatments became more pronounced (Fig. A.13, s.m.). For FW samples A, B, C, and G the infiltration fronts were very sharp and mostly stable for the first 80 min. After that, they became slightly unstable. At the end of the experiment, except for sample G, all FW samples were uniformly and homogeneously wetted. In contrast, under TWW irrigation the instabilities of the infiltration front occurred already after 40 min to 80 min for all samples. In a depth of 20 min to 50 min the infiltration fronts propagation stopped and water flowed through single path ways to the lower boundary. At sample I, L, N, and O, large areas with no change in water content were detected.

Patterns of water infiltration at the end of the experiment were quantified via a threshold of $\overline{\Delta\theta} - 3{*}sd$. Fig. 7 shows the reduction of used area for the samples due to the drying process as a relative value of the projected sample area. After three days of drying the median of TWW flow fields was reduced to 86.1% of the projection area, after seven days to 50.4%. Whereas for FW samples the area used for water flow did not significantly change due to drying. Changes in absolute soil water holding capacities at this specific infiltration rate were determined by gravimetric data. Fig. 8 illustrates the relation of water loss through drying to water gain by infiltration, so called rewetting ratio. Thus, the water content after irrigation at field moisture was used as reference. The rewetting ratios of 1 as obtained for the completely wettable samples confirmed the validity of this approach. The determined ratios show that the capacity of TWW samples for water uptake was reduced by the drying process. After three days the median rewetting ratio of TWW samples was reduced to 0.83, after seven days to 0.57. FW samples re-established their water contents after three days (1.08) and after seven days (0.94). Some samples slightly increased their water contents (rewetting ratio $> 1$) due to the change of the lower boundary from gravity flow to seepage. A statistical analysis (ANOVA, Tukey multiple comparisons of means, $\alpha = 5$ %) provided a significant difference in the rewettability between FW and TWW treatment after seven days ($p < .05$), but not after three days.

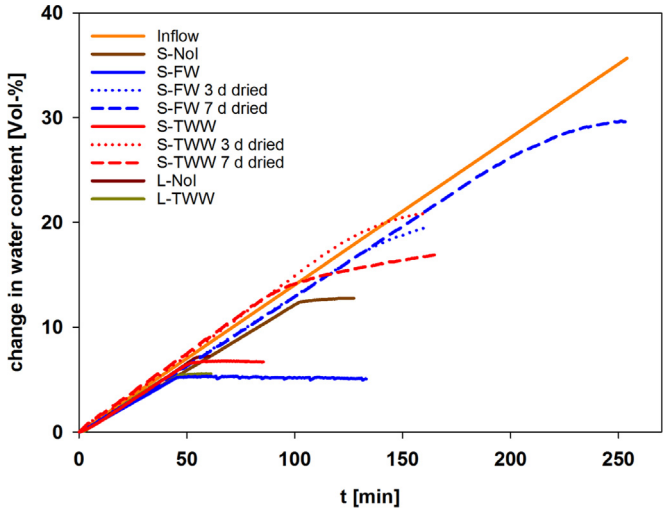


**Fig. 6.** Gravimetric changes in water content $\Delta\theta$ (vol %) as a function of time for all presented samples.

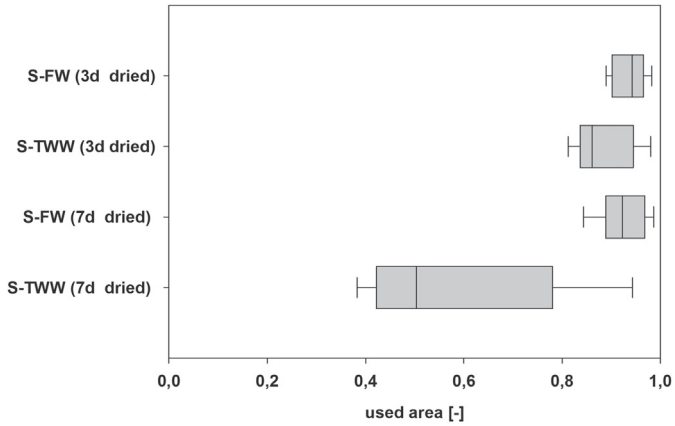


**Fig. 7.** Relative area of $\Delta\theta$ within a 99.8% confidence interval of water flow.

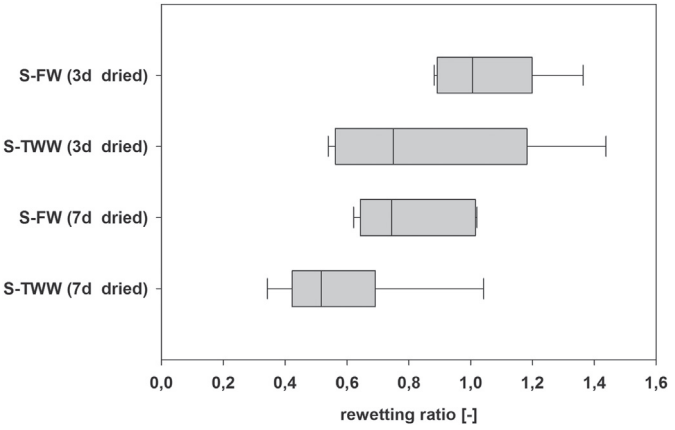


**Fig. 8.** Capacity of the sample to reach the water content of the completely wetted initial experiment.

## 4. Discussion

Soil water repellency was detected for all sampling locations except for S-NoI, independent of the season, irrigation treatment or soil texture, but with variation in severity and frequency of occurrence. While FW samples in Rehovot (loamy sand) provided a seasonal dynamic in hydrophobicity, water repellency at TWW irrigation plots were not reduced by rain. Hydrophobicity seems to have become a persistent soil characteristic under TWW irrigation. Furthermore, for loamy sand the initial contact angles close to soil surface were significantly increased by TWW irrigation compared to FW plots. However, as FW plots were irrigated from 2008 to 2012 with TWW, the topsoil was still classified as water repellent.

By comparing the decrease of CA with time, it has been shown that the persistence of water repellency in TWW plots was two to four times larger than in FW plots, especially at larger depths. Three years of 700 mm FW irrigation and 550 mm of precipitation were not sufficient to turn the soil hydrophilic, but changed the persistence of repellency. The sandy clay loam in Hadera provided different results. Here, soil under TWW irrigation was mostly defined as wettable to slightly water repellent and the analysis of CA showed a significant reduction of repellency at the end of rainy season. Moreover, the non-irrigated part was significantly more affected by water repellency at the end of the winter than the irrigated part at all season, and provided by far the highest CA at the soil surfaces of all measurements.

By analysing water repellency of the single layers it has been shown that hydrophobicity detected by WDPT in samples taken under irrigation (FW and TWW) was equally distributed over the entire sampling depth, whereas in L-NoI repellency concentrated in the top layers and decreased with depth. This was confirmed by the dynamic CA measurements which decreased more rapidly with depth. Compared to the other treatments a higher amount of litter and humic substances with local heterogeneities were observed in the upper 30 mm of L-NoI which was covered with leafs at all season. Besides the organic input by TWW irrigation, hydrophobicity can be established by other organic materials such as input of organic litter from citrus trees, which contain waxes and other amphipathic substances (González-Peñaloza et al., 2012; Scott, 2000; Zavala et al., 2009). Furthermore, in summer 2015 patterns of moist soil were leading from the drippers to the non-irrigated rows, which indicates an impact of TWW to L-NoI. In Hadera, the irrigated part of the orchard is kept moist over the year, therefore the micro-biological activity is probably higher as compared to the non-irrigated part where degradation of organic substances can be reduced by limitation of water. Water repellency detected in L-NoI can be explained by a combination of accumulation of organic material with high contents of amphiphilic substances and surface run-off from TWW irrigated plots. Here, a more detailed look into the distribution of organics, their characteristics, and their occurrence inside soil structure is needed to determine their sources and appearances, which is beyond the scope of the current study.

The potential water repellency was measured at dried soil comparable to the seven days dried samples of the infiltration test series. Our experiments mimicked different field conditions in terms of initial water content. The field moist samples of both study sites mainly showed a homogeneous propagation of water infiltration fronts and an increase in water content over the entire sample heights. For the sandy clay loam, the NoI samples provided some slight heterogeneities in flow pattern. Here, local heterogeneities of organic material in the topsoil might have influenced the capacity of water uptake and water flow. It should be noticed that field moist samples from Hadera were close to saturation behind the infiltration front and therefore larger macro-pores were probably activated and dominated water distribution.

At both study sites, some samples showed a decreasing change in water content from top to bottom or areas with low changes. This can be attributed to the high initial water content with a water gradient along the sample height due to gravity, and to local heterogeneities in soil density. In this case, little changes in water content are required to conduct the applied water flux. Hence, small variabilities in density can have a considerable influence on the detection of the flow field since our method is only sensitive to changes in water content. Furthermore, changes of soil structure e.g. due to shrinking and swelling of clay

minerals or particle transport might be interpreted as changes in water content (sample I Fig. A.11, s.m.). Nevertheless, even small changes in water content were captured for the entire sample areas of all field moist samples which could be confirmed by gravimetric measurements.

No preferential flow was detected for field moist soil, independent of the water quality and the season. An exception was sample J (S-FW) where water flow was dominated by layering of different soil textures. In contrast to field moist samples, uneven wetting front propagation and preferential flow was detected for most of the TWW samples from Rehovot after reducing the soil water content to 13 vol %. This was not the case for FW samples. After seven days of drying (1.5 vol %) the influence of the long-term irrigation of TWW became even more severe, as large areas of the samples were excluded from water flow and staid dry. The analysis of gravimetric data supports these findings, as the rewetting capacity of TWW was reduced in average about 12% and 27%, one sample even lost 59% of water storage capacity. These results confirm the findings of other studies where water repellency was found to be closely linked to low initial water contents (Bauters et al., 2000; Wallach and Jortzick, 2008; Xiong et al., 2012). No systematic characteristic of flow fields was observed, they were highly individual. It is noted that the FW samples from October were classified as strongly water repellent, similar to TWW samples, which, however, did not influence the infiltration propagation. The persistence of water repellency measured by CA dynamics may explain this phenomenon as CA measured for FW samples were decreasing much faster than for TWW, especially in the detected critical zone of 20 min to 50 min. Here, the reorientation of hydrophobic molecules by water seems to be fast enough to enable a more homogeneous wetting of the samples.

## 5. Conclusion

Long-term treated waste water irrigation causes potential water repellency in soils. Its severity is dependent on soil texture and its effect on water infiltration is more pronounced when soil is dry. In soil column experiments, we found that the presence of water repellency may not be a noticeable problem for water dynamics as long as the soil is kept moist. Once soil is exposed to water shortage, the risk of preferential flow, surface run-off, and reduced water storage increases severely. For a loamy sand irrigated with TWW for more than five years, it was clearly shown that water flow became highly preferential when water contents drop below some 13 vol %. By using the new approach to detect changes in water content via X-ray radiography, it was possible to quantify the spatial pattern of infiltration fronts in undisturbed, cylindrical soil cores. This provides more substantial information on the heterogeneity of water flow as compared to chemical tracers or by using quasi-two-dimensional Hele-Shaw cells. Moreover, we could demonstrate that measurement of the dynamic contact angle is a useful parameter to explain the occurrence of different flow regimes in dry samples which were classified as water repellent by water drop penetration time and initial contact angle.

## Acknowledgments

This work was supported by the German Federal Ministry of Food and Agriculture (FKZ: 2813IL04) and partially by the Israel Ministry of Agriculture. It is part of the project “ Impact of effluent irrigation on soil water dynamics and sustainable land use: Synergistic effects of altered soil structure and wettablility”. We thank G. Lerner for his help during field work, S. Kruk for the laboratory study in Israel, Dr. M. Koehne for technical support, and the orchards management for providing their field sites.

## Appendix A. Supplementary data

The following figures show changes in water content (vol %) during infiltration experiments of all field moist soil columns from Rehovot (loamy sand) and Hadera (sandy clay loam), and from the experiment with reduced initial water contents. The columns of the figures separate samples from different sampling points and treatments, the rows show the progress of infiltrating water after certain time steps. Individual exceptions of time steps (designated with additional times) were chosen for better illustration of the infiltration front. Figs. A.9 and A.10 show results of Rehovot, A.11 of Hadera, Figs. A.12 and A.13 of the drying experiment. In Rehovot column S and T are the results of 20 cm height samples, in Hadera columns G and J. Supplementary data to this article can be found online at https://doi.org/10.1016/j.geoderma.2018.01.004.

## References

Allaire, S.E., Roulier, S., Cessna, A.J., 2009. Quantifying preferential flow in soils: a review of different techniques. J. Hydrol. 378 (1), 179–204.
Bachmann, J., Ellies, A., Hartge, K.H., 2000. Development and application of a new sessile drop contact angle method to assess soil water repellency. J. Hydrol. 231–232, 66–75.
Bauters, T., Steenhuis, T., DiCarlo, D., Nieber, J., Dekker, L., Ritsema, C., Parlange, J.-Y., Haverkamp, R., 2000. Physics of water repellent soils. J. Hydrol. 231, 233–243.
Bisdom, E., Dekker, L., Schoute, J.T., 1993. Water repellency of sieve fractions from sandy soils and relationships with organic material and soil structure. Geoderma 56 (1–4), 105–118.
Bughici, T., Wallach, R., 2016. Formation of soil-water repellency in olive orchards and its influence on infiltration pattern. Geoderma 262, 1–11.
Carrillo, M.L.K., Letey, J., Yates, S.R., 2000. Unstable water flow in a layered soil II. Effects of an unstable water-repellent layer. Soil Sci. Soc. Am. J. 64 (2), 456–459.
Clothier, B.E., Vogeler, I., Magesan, G.N., 2000. The breakdown of water repellency and solute transport through a hydrophobic soil. J. Hydrol. 231–232, 255–264.
DeBano, L.F., 1981. Water repellent soils: a state-of-the-art. Gen. Tech. Rep. PSW 46.
Dekker, L.W., Ritsema, C.J., 1994. How water moves in a water repellent sandy soil: 1. Potential and actual water repellency. Water Resour. Res. 30 (9), 2507–2517.
Dekker, L.W., Ritsema, C.J., 2000. Wetting patterns and moisture variability in water repellent Dutch soils. J. Hydrol. 231–232, 148–164.
Doerr, S.H., 1998. On standardizing the ‘water drop penetration time’ and the ‘molarity of an ethanol droplet’ techniques to classify soil hydrophobicity: a case study using medium textured soils. Earth Surf. Process. Landf. 23 (7), 663–668.
Doerr, S.H., Ritsema, C.J., Dekker, L.W., Scott, D.F., Carter, D., 2007. Water repellence of soils: new insights and emerging research needs. Hydrol. Process. 21 (17), 2223–2228.
Doerr, S.H., Shakesby, R.A., Walsh, R.P.D., 2000. Soil water repellency: its causes, characteristics and hydro-geomorphological significance. Earth Sci. Rev. 51 (1–4), 33–65.
González-Peñaloza, F.A., Cerdà, A., Zavala, L.M., Jordán, A., Giménez-Morera, A., Arcenegui, V., 2012. Do conservative agriculture practices increase soil water repellency? A case study in citrus-cropped soils. Soil Tillage Res. 124, 233–239.
Graber, E., Tagger, S., Wallach, R., 2007. Do surface active substances from water repellent soils aid wetting? Eur. J. Soil Sci. 58 (6), 1393–1399.
Horne, D.J., McIntosh, J.C., 2000. Hydrophobic compounds in sands in New Zealand — extraction, characterisation and proposed mechanisms for repellency expression. J. Hydrol. 231–232, 35–46.
Kobayashi, M., Shimizu, T., 2007. Soil water repellency in a Japanese cypress plantation restricts increases in soil water storage during rainfall events. Hydrol. Process. 21 (17), 2356–2364.
Kuka, K., Illerhaus, B., Fritsch, G., Joschko, M., Rogasik, H., Paschen, M., Schulz, H., Seyfarth, M., 2013. A new method for the extraction of undisturbed soil samples for X-ray computed tomography. J. Nondestruct. Test. 2013 (8).
Lado, M., Ben-Hur, M., 2009. Treated domestic sewage irrigation effects on soil hydraulic properties in arid and semiarid zones: a review. Soil Tillage Res. 106 (1), 152–163.
Letey, J., Carrillo, M., Pang, X., 2000. Approaches to characterize the degree of water repellency. J. Hydrol. 231, 61–65.
Lipsius, K., Mooney, S.J., 2006. Using image analysis of tracer staining to examine the infiltration patterns in a water repellent contaminated sandy soil. Geoderma 136 (3), 865–875.
OECD, 2015. Water Resources Allocation. OECD Publishing.
Rahav, M., Brindt, N., Yermiyahu, U., Wallach, R., 2017. Induced heterogeneity of soil water content and chemical properties by treated wastewater irrigation and its reclamation by freshwater irrigation. Water Resour. Res. 53 (6), 4756–4774.
Rye, C.F., Smettem, K.R.J., 2017. The effect of water repellent soil surface layers on preferential flow and bare soil evaporation. Geoderma 289, 142–149.
Scott, D., 2000. Soil wettability in forested catchments in South Africa; as measured by different methods and as affected by vegetation cover and soil characteristics. J. Hydrol. 231, 87–104.
Wallach, R., Ben-Arie, O., Graber, E.R., 2005. Soil water repellency induced by long-term irrigation with treated sewage effluent. J. Environ. Qual. 34 (5), 1910–1920.
Wallach, R., Jortzick, C., 2008. Unstable finger-like flow in water-repellent soils during wetting and redistribution — the case of a point water source. J. Hydrol. 351 (1–2), 26–41.
Wang, Z., Wu, Q., Wu, L., Ritsema, C., Dekker, L., Feyen, J., 2000. Effects of soil water repellency on infiltration rate and flow instability. J. Hydrol. 231, 265–276.

Weller, U., Leuther, F., Schlueter, S., Vogel, H.-J., 2017. Quantitative analysis of water infiltration in soil cores using X-ray. Vadose Zone J.
Weller, U., Vogel, H.J., 2012. Conductivity and hydraulic nonequilibrium across drainage and infiltration fronts. Vadose Zone J. 11 (3).
Xiong, Y., Furman, A., Wallach, R., 2012. Moment analysis description of wetting and redistribution plumes in wettable and water-repellent soils. J. Hydrol. 422, 30–42.
Zavala, L.M., González, F.A., Jordán, A., 2009. Intensity and persistence of water repellency in relation to vegetation types and soil parameters in Mediterranean SW Spain. Geoderma 152 (3–4), 361–374.